Published online: March 30, 2020

IMR Press

Original Research

EEG effective connectivity networks for an attentive task requiring vigilance based on dynamic partial directed coherence

Songyun Xie[1] and Yabing Li[2,*]

[1]*NPU-TUP Joint Laboratory for Neural Informatics, Northwestern Polytechnical University, Xi'an, Shaanxi Province, 710129, P. R. China*

[2]*School of Computer Science and Technology, Xi'an University of Posts and Telecommunications, Xi'an, Shaanxi Province, 710121, P. R. China*

*Correspondence: liyabing@xupt.edu.cn (Yabing Li)

DOI:10.31083/j.jin.2020.01.1234

An effective network perspective focused on measuring directional interactions of electroencephalographic in different cortical regions during a sustained attentive task requiring vigilance. A novel measure referred to as dynamic partial directed coherence was used to map the cognitive state of vigilance based on graph theory. In the right parieto-occipital area, the area is significantly higher than in other regions of interest (the areas are 0.601 and 0.632 for out-degree and in-degree, respectively). A similar analysis in the right fronto-central area revealed significant differences in the different cognitive states. Across the six regions of interest, significant differences of in-degree and out-degree based alpha band are observed in the right fronto-central and the right parieto-occipital ($P < 0.05$). The performance was compared with those from a support vector machine using different network-based phase-locking values, partial directed coherence, and dynamic partial directed coherence. Results show that dynamic partial directed coherence can provide more information about direction (compared with phase-locking values) and accuracy (when compared with partial directed coherence). The graph theoretical analysis shows that the effective network based dynamic partial directed coherence has a small-world property for synchronizing neural activity between brain regions. Moreover, the alpha band is well correlated with the cognitive state compared to other frequency bands.

Keywords

Effective network; fronto-central; right parieto-occipital; cortex; electroencephalographic; partial directed coherence; graph theory; cognitive models; attention; vigilance

1. Introduction

Recent work analyzed the brain network based on graph theory (Gorban and Zinovyev, 2010). and how it can exert its sensory and cognitive functions (Omidvarnia et al., 2014). Neuroimaging has been an experimental tool for network neuroscience for more than two decades. Dimitriadis et al. (2012) used the concept of commute times (CTs) to investigate the interplay of network and showed that CTs could be used to track the dynamics of the brain's functional organization. da Fontoura Costa and Sporns (2006) segregated brain regions to model the complex network and demonstrated that it had a strong correlation between network features based on graph theory (in and out-degree) and dynamic features of cortical activation. Gonuguntla et al. (2016) analyzed the network pattern related to cognitive function based on the phase-locking value (PLV) and electroencephalographic (EEG) data for motor imagery; the results indicated that the proposed method could achieve better classification performance compared to band-power-based approaches for single-trial analysis. Omidvarnia et al. (2011) quantified the connectivity between cortical brain regions and demonstrated that time-varying *partial directed coherence* (PDC) of cortical connectivity could lead to a better understanding of cognitive function.

The brain network connections are modeled as nodes and edges (Rubinov and Olaf., 2010). The degree, as one of the basic and vital measures, can reflect the importance of nodes in the network. The characteristic of path length is known as the average shortest path length between all of the pairs of nodes in the network, and it can be used to represent a measure of effective integration. The clustering coefficient is a measure of local network connectivity that shows 'small-world' property for synchronizing neural activity between different brain regions (Ferri et al., 2007; Stam et al., 2007).

Vigilance or sustained attention is one of the most significant cognitive functions in long-term monitoring for monotonous attention-demanding (Akin et al., 2008). Due to the lack of reliable techniques, it is challenging to map brain regions associated with vigilance. The purpose of this paper is to investigate whether it is possible to identify brain regions responsible for vigilance using electroencephalography (EEG) signals. The method combines graph theory with PDC to analyze the functional connectivity network and monitor changes in vigilance state associated with special bands.

Journal of Integrative Neuroscience

2. Materials and methods

2.1 Participants

A total of thirteen healthy subjects were collected in this experiment (average age of 23.23 $\pm$ 1.30 years old; 8 males and 5 females). All of the subjects are right-handed and have a standard or corrected-to-normal vision, with no sleep problem or alcohol abuse. Also, subjects with neurological and psychological disorders were excluded from this study (Funke et al., 2010).

Before the experiment, the experimental material was introduced to the subjects. The subject was then asked to practice the task in the experimental procedures for 10 mins. The NASA Task Load Index (NASA-TLX), which is one of the most effective and widely used indices, was used to measure the mental workload. It has a 0-100 scale and six subscales (mental demand, physical demand, temporal demand, performance, effort, and frustration) (Hart and Staveland, 1988). To measure the effects of workload on vigilance or sustained attention, the NASA-TLX of subjects was collected before and after the experiment, respectively (Finomore et al., 2013).

2.2 Experiment

An air traffic controller task was used as a vigilance task. Concentric circles divided into four quadrants were displayed on the computer. Four planes of random directions were placed into four quadrants, as shown in Fig. 1A. In a safety situation (non-target), the aircraft were all oriented in the same direction: in the collision situation (target), planes were in opposite directions.

For the vigilance task, participants were asked to monitor the computer screen and respond to the target stimulus. The stimulus was presented for 1 s, with an inter-stimulus interval (ISI) between 1 s and 9 s randomly, as shown in Fig. 1B. The stimulus was updated 100 times for each session, and one epoch means one updated time for the stimulus (the duration of time is 4 s: 2s before and after stimulus occurred). The ratio between target and non-target stimuli was 1:4 throughout the task, which means that the probability of encountering a target stimulus was 20%. The hit rate, which can be used to monitor the vigilance state of a subject, indicated the likelihood of a subject responds 'yes' in a collision situation and defined as:

$$hit\ rate = \frac{right_{response}}{Stimulus_{num}} \tag{1}$$

where $Stimulus_{num}$ is the total number of stimulus in each session and $right_{response}$ is the right response to a stimulus. The vigilance level was mapped into three levels according to the hit rate. The hit rate of 0-0.5 was assigned to" negative," "neutral" was equal to 0.5-0.7, and 0.7-1 was" positive."

2.3 Data acquisition and pre-processing

The EEG data were recorded using a GES 300 System (EGI product. Sensor array: 64-channel adult-sized head cap). The EEG acquisition software was Net Station (Computer: Power PC G5; amplifier: Net Amps 300). The EEG signals were acquired by the 10-20 system, which is an international system to ensure standardized reproducibility. Moreover, the raw EEG signal was sampled at 250Hz and band-pass filtered between 1Hz and 40Hz. The bad trials, which contained noticeable artifacts (eye blink, eye movement, and electromyography (EMG)), were excluded.

After removing the artifacts, each epoch was filtered in the delta [$<$ 4Hz], theta [4-8Hz], alpha [8-13Hz], and beta [13-30Hz] bands. The EEG signals were averaged in 6 ROIs for the next step (Charbonnier et al., 2016), as shown in Fig. 2.

2.4 Methods

EEG effective connectivity networks represent the direct or indirect causal influences from one region to another, defined by a collection of nodes and edges. Nodes in the effective network represent different brain regions, while edges represent the connections between pairs of nodes

Partial and directed relationships can be quantified using the PDC measurement, which determines directional influence in multivariate systems. For example, assuming that ROI1 influences by ROI2 and ROI2 influences ROI3, we can express using ROI2$\leftarrow$ ROI1, ROI3$\leftarrow$ ROI2. Here, the arrows show the direction of the information flow. In this example, ROI1 has a direct influence on ROI2, while there is an indirect (partial) influence between ROI1 and ROI3.

We employed PDC and its modified method to construct the brain network. PDC is defined as:

$$\mathrm{PDC} = \begin{bmatrix} \pi_{11} & \cdots & \pi_{16} \\ \vdots & \ddots & \vdots \\ \pi_{61} & \cdots & \pi_{66} \end{bmatrix} \tag{2}$$

where 6 is the total number of regions or channels in the EEG signals. In this network, $\pi_{ij}$of the network tabulates the strength of effective connectivity between regions *i* and *j*. A PDC of zeros indicts that the connectivity of two regions is independent, while a PDC of one means that the connectivity of two regions is stable.

In the PDC matrix π_{ij} in Eqn. 2 is defined as follows:

$$\pi_{ij}(f) = \frac{\bar{A}_{ij}(f)}{\sqrt{\bar{a}_j^H(f)\,\bar{a}_i(f)}} \tag{3}$$

$$\bar{A}_{ij}(f) = \begin{cases} 1 - \sum_{r=1}^{p\_order} a_{ij}(r)\, e^{-2\pi f r} & if \quad i = j \\ -\sum_{r=1}^{p\_order} a_{ij}(r)\, e^{-2\pi f r} & otherwise \end{cases} \tag{4}$$

where $\bar{a}_i$ is the *i*th column of $\bar{A}_{ij}$. π_{ij}, which can be obtained from Eqn. 3 and Eqn. 4, is the instantaneous effective relationship in measure-specific between a pair of regions. The frequency *f* varies within the range of 0 to 1/2 of the Nyquist rate. The higher the value of π_{ij}, the greater the strength in the connectivity from region *i* to *j*.

As well the processed EEG signal with the ROIs index:

$$\begin{bmatrix} x_1(n) \\ \vdots \\ x_6(n) \end{bmatrix} = \sum_{r=1}^{p_{\text{order}}} \begin{bmatrix} a_{11}(r) & \cdots & a_{16}(r) \\ \vdots & \ddots & \vdots \\ a_{61}(r) & \cdots & a_{66}(r) \end{bmatrix} \begin{bmatrix} x_1(n-r) \\ \vdots \\ x_6(n-r) \end{bmatrix} + \begin{bmatrix} w_1(n) \\ \vdots \\ w_6(n) \end{bmatrix} \tag{5}$$

where the real-valued parameter $a_{ij}(r)$ reflects the linear rela-

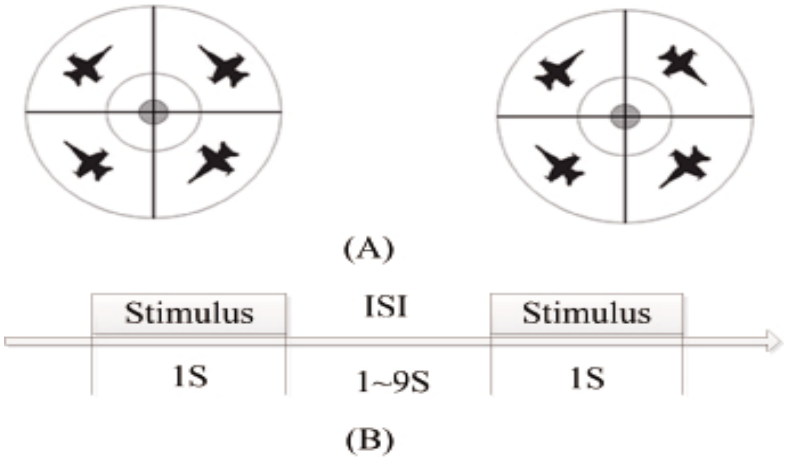

Figure 1. The experimental paradigm. (A) Examples of flying events, the first indicates the plane in the collision situation; the second suggests the plane in a safe position. (B) Schematic design of the experimental conditions.

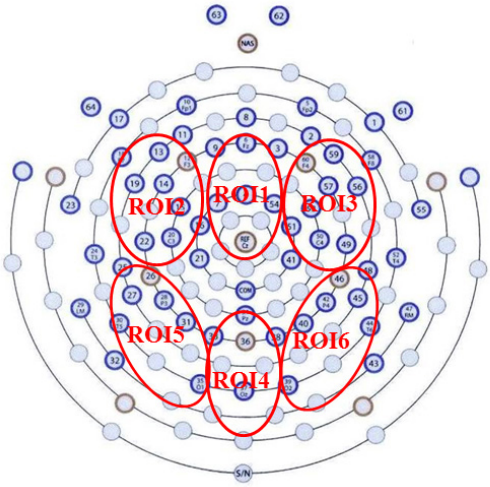

ROI1 Fronto-Central median: Fz, Cz, Fc1, Fc2

ROI2 Fronto-Central left: F7, F3, Fc5, C3

ROI3 Fronto-Central right: F4, F8, Fc6, C4

ROI4 Parieto-Occipital median: Pz, Poz, Oz

ROI5 Parieto-Occipital left: Cp5, P3, P7, O1

ROI6 Parieto-Occipital right: Cp6,P4,P8,O2

Figure 2. ROIs for 64-channel adult-sized head cap. ROI1 consists of the channels of Fz, Cz, Fc1, and Fc2; ROI2 consists of the channels of F7, F3, Fc5, and C3; ROI3 consists of the channels of F4, F8, Fc6, and C4; ROI4 consists of the channels of Pz, Poz, and Oz; ROI5 consists of the channels of Cp5, P3, P7, and O1; ROI6 consists of Cp6, P4, P8, and O2.

tionship between regions i and j at the delay r, w is a normally distributed White noise. Considering the simplicity factors, the optimum order *p_order* of an MVAR model is estimated using Schwartz-Bayesian Criterion (SBC) (Neumaier and Schneider, 2001).

The energy of a specific frequency band in which the PDC of EEG signals show significant variations between the different cognitive states is called the reactive band. The variations in the reactive band of EEG in vigilance analysis always select alpha, beta, theta, and delta waves. In this paper, the reactive band was used to analyze the vigilance states-based PDC network of measure-specific for all of the regions in the band of interest. The dPDC represents the difference between cognitive and reference states, and can be defined as:

$$\mathrm{dPDC}_{specific} = \mathrm{PDC}_{cognitive} - \mathrm{PDC}_{reference} \qquad (6)$$

where $\mathrm{PDC}_{cognitive}$ represents the average PDC in the band of interest (for example delta, theta, alpha, and beta band) during the cognitive period duration, and $\mathrm{PDC}_{reference}$ is the average PDC during the reference period duration (the first 1.25s before stimulus occurred during the experiment).

According to Eqn. 6, $\mathrm{dPDC}_{specific}$is computed for all of the region pairs of subject's cognitive states in a specific band. The analysis of $\mathrm{dPDC}_{specific}$ and frequency band provide chances to identify the cognitive-related reactive band. One of the main limitations in the analysis of spatial EEG is the effect of volume conduction, which can be minimized using dPDC.

The weak edges of brain networks tend to obscure the topology of strong connections, so these edges are often discarded using an appropriate weight threshold. Once the weight between edges is below the weight threshold level, all of the connections must be removed or discarded before analysis. Numerous methods have been proposed to set the threshold for the network; nevertheless, there is no general procedure available to set a proper threshold we

set to ensure the networks have the same density:

$$\begin{aligned} Num &= prob \cdot 36 \\ Series &= sort(\text{dPDC}) \\ threshold &= Series_{Num} \end{aligned} \tag{7}$$

where 'prob' is the connectivity probability of network, which means the rate between connectivity edges and the whole edges for the network' '36' represents the number of pairs between regions, and the value of dPDC is the weights between nodes of the network. An effective network can be built by using the threshold (above the threshold keeps the original value, and below the threshold is set to zero).

2.5 Graph theory characters of effective network

To analyze and characterize a network between different regions, we employed dPDC measurement. In this section, we calculated the characteristics of dPDC using graph theory for the connectivity graph.

The degree (Rubinov and Olaf., 2010) for each node reflects the importance in the network, which is equal to the number of nodes that connected to that node. Note that network based dPDC is a directed network, and it can be divided into in-degree and out-degree. The in-degree represents the number of inflows from neighbors, while out-degree represents the number of outflows, as defined as:

$$\begin{aligned} k_i^{out} &= \sum\nolimits_{j \in N} matrix_{ij} \\ k_i^{in} &= \sum\nolimits_{j \in N} matrix_{ji} \end{aligned} \tag{8}$$

where N is the set of all nodes in the network, and $matrix_{ij}$ is the parameter of a network between regions i and j, and k_i^{out} and k_i^{in} is the out-degree and in-degree for the i-th node, respectively.

The clustering coefficient (C) (Fagiolo, 2007), which is known as the fraction of triangles around an individual node, can also be defined as the rate between the node's neighbor and the others. It describes the interconnected density groups of nodes and is defined as follows:

$$C = \frac{1}{n} \sum_{i \in N} \frac{S_i}{\left(k_i^{out} + k_i^{in}\right)\left(k_i^{out} + k_i^{in} - 1\right) - 2\sum_{j \in N} matrix_{ij} matrix_{ji}} \tag{9}$$

where S_i can be obtained from:

$$\begin{aligned} S_i = \frac{1}{2} \sum_{j,h \in N} &\left(matrix_{ij} + matrix_{ji}\right) \\ &\left(matrix_{ih} + matrix_{hi}\right)\left(matrix_{hj} + matrix_{jh}\right) \end{aligned} \tag{10}$$

The shortest path length (L) reflects the ease with information communication of brain regions. The shorter the L is, the stronger the communication ability of brain regions has. So, this character can be more natural to interpret efficiency on connected networks. It can be defined as:

$$d_{ij} = \sum\nolimits_{matrix_{uv} \in g_{i \to j}} matrix_{uv} \tag{11}$$

where $g_{i \to j}$ the directed shortest path between i and j, $matrix_{uv} \in g_{i \to j}$means that the connectivity between u and v belongs to the part of $g_{i \to j}$.

2.6 Statistical analysis

To evaluate our experiment, we used linear correlation analysis and t-test as the evaluation criteria. Linear correlation analysis was performed to analyze the relationship between NASA-TLX score and hit rate. For the frequency-specific reactive band, a t-test was used to establish a significant difference between positive and negative vigilance state. The level of significance was set at $P < 0.05$.

3. Results

3.1 The relationship between hit rate and NASA-TLX scores

In Fig. 3, we illustrate the hit rate (the accuracy of correct response for stimulus) and NASA-TLX scores in thirteen healthy subjects. Overall, there was a reverse tendency between NASA-TLX scores and different vigilance states of subjects. NASA-TLX score indicated the overall workload on 6 scales (physical demands, temporal demands, performance, effort, frustration) in subjects. S11 achieved the highest score of NASA-TLX (around 67 scores) and the lowest score of hit rate (about 60%). The results demonstrated that subjects' workload had significant effects on hit rate, with a slope of about -1.26, which represented the extent of the linearity relationship. It is noticed that the hit rate was negatively correlated with the NASA-TLX scores ($P < 0.05$) with an r-value of -0.875.

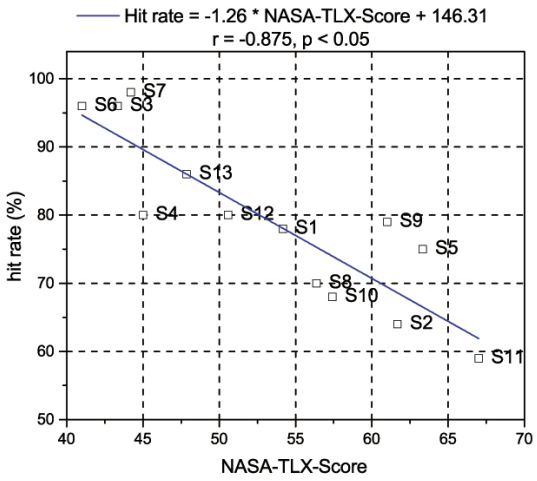

Figure 3. Linear correlation of the estimated parameters with NASA-TLX score and hit rate. NASA-TLX score means the overall workload on six scales (physical demands, temporal demands, performance, effort, frustration); the hit rate represents a correct response to a stimulus. From the figure, the hit rate is negatively correlated with workload using linear regression (r = -0.875). The negative value of slope represents adverse, and the absolute value of slope represents the extent of the impact between workload and hit rate (slope = -1.26).

3.2 The parameters estimation for modeling the network

To select the optimal order (*P order*) of SBC for the MVAR model (see §2 Methods), we analyzed the relationship between order and SBC measures for different cognitive states. The results were shown in Fig. 4, and the order at 5, which minimized the SBC

Table 1. Significance test for 'in-degree' with the positive vigilance group and the negative vigilance group at four frequencies in six ROIs (T is the t value for student's t test and *P* is the level of statistical significance).

In-degree	Alpha		Beta		Theta		Delta	
	T	*P*	T	*P*	T	*P*	T	*P*
ROI1	**-2.826**	**0.007**	-0.518	0.607	-1.856	0.07	-0.53	0.599
ROI2	0.338	0.736	1.096	0.279	0.338	0.737	0.213	0.832
ROI3	**2.124**	**0.039**	-1.856	0.07	-1.737	0.089	**-2.145**	**0.038**
ROI4	1.45	0.154	-1.737	0.089	1.45	0.154	1.604	0.116
ROI5	-0.784	0.437	-1.198	0.238	-0.784	0.437	-0.229	0.819
ROI6	**2.886**	**0.006**	0.813	0.421	**2.886**	**0.006**	1.262	0.214

measures, was selected for further analysis. After the parameters of the order were determined, the PDC brain network was obtained by using the parameters of the MVAR model.

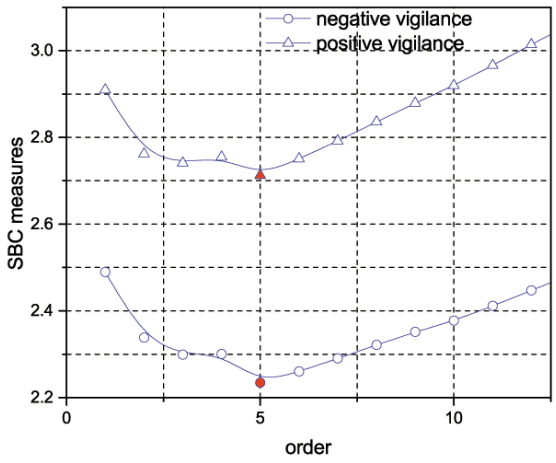

Figure 4. The relationship between order and SBC measures. B-Spline non-linear curve was used. The order ranger was from 1 to 13, and the order at 5 (the minimum of the SBC measures) was selected.

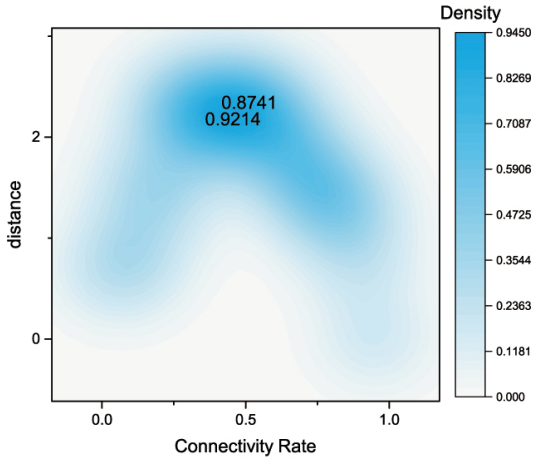

Figure 5. The 2D kernel density plot is a smoothed color density representation of the scatter plot based on kernel density estimation. It shows the relationship between connectivity rate and distance. The network density is calculated with connectivity rate ranges from 5% to 95%, with an increment of 5%. To determine the optimal threshold, the maximum of the density is selected as indicated (the threshold for connectivity rate is 0.4).

For a low value of the threshold, the network was connected with edges between almost all of the nodes leading to the network density (close to 1). With the threshold values were increased, more and more edges were lost, and the clustering coefficient was decreased. The network density was selected using a traversal algorithm (threshold values ranging from 5% to 95% with an increment of 5%) until maximized distance differences between the cognitive states, as shown in 0. It is noted that the higher the density is, the further is the distance with the threshold (the parameter of probability in Eqn. 7) given by 0.4.

3.3 Selection of the frequency-specific reactive band

Independent sample t-tests of 'in-degree' and 'out-degree' between positive and negative vigilance states for each network-based frequency band and ROI presented in Table 1 and Table 2.

For in-degree, independent sample t-tests showed there were significant difference for dPDC based alpha band between positive and negative vigilance states in special ROIs (ROI1 (t = -2.826, *P* = 0.007), ROI3 (t = 2.124, *P* = 0.039) and ROI6 (t = 2.886, *P* = 0.006)). Moreover, the statistical analysis had given a significant difference in ROI6 (t = 2.886, *P* = 0.006) for dPDC based theta band and ROI3 (t = -2.145, *P* = 0.038) for delta band while t-test showed no significant differences for the dPDC for others.

For out-degree, statistical analysis showed there was a significant difference for dPDC based alpha band between positive and negative vigilance states in special ROIs (ROI1 (t = -2.383, *P* = 0.022), ROI3 (t = 2.752, *P* = 0.009) and ROI6 (t = -2.519, *P* = 0.016)) were significant. Moreover, the statistical analysis also showed there was a significant difference in special ROIs (ROI1, ROI3, and ROI6) for dPDC based theta band, ROI1, and ROI3 for the delta band and in ROI3 for the beta band while t-test showed no significant differences for the dPDC for others.

To visualize the performance for different ROIs, the receiver operating characteristics (ROC) graphs of 'in-degree' and 'out-degree' characters based alpha band in distinguishing positive vigilance state from negative vigilance were shown in Fig. 6 and Table 3. In the right parieto-occipital (ROI6), the area under the curve was significantly higher than that in the other ROIs (the areas were 0.601 and 0.632 for 'out-degree' and 'in-degree,' respectively). A similar analysis in the right fronto-central (ROI3) re-

Table 2. Significance test for 'out-degree' with the positive vigilance group and the negative vigilance group at four frequencies in six ROIs (T is the t value for student's t test and *P* is the level of statistical significance).

Out-degree	Aalpha		Beta		Theta		Delta	
	T	*P*	T	*P*	T	*P*	T	*P*
ROI1	**-2.383**	**0.022**	-1.746	0.088	**-2.383**	**0.022**	**-3.022**	**0.004**
ROI2	-0.199	0.842	-0.904	0.371	-0.199	0.843	0	1
ROI3	**2.752**	**0.009**	**3.101**	**0.003**	**2.752**	**0.008**	**3.149**	**0.003**
ROI4	0.984	0.331	-1.475	0.148	0.984	0.331	0.481	0.633
ROI5	0.404	0.688	1.936	0.059	0.404	0.688	0.304	0.762
ROI6	**-2.519**	**0.016**	-1.898	0.064	**-2.519**	**0.016**	-1.836	0.073

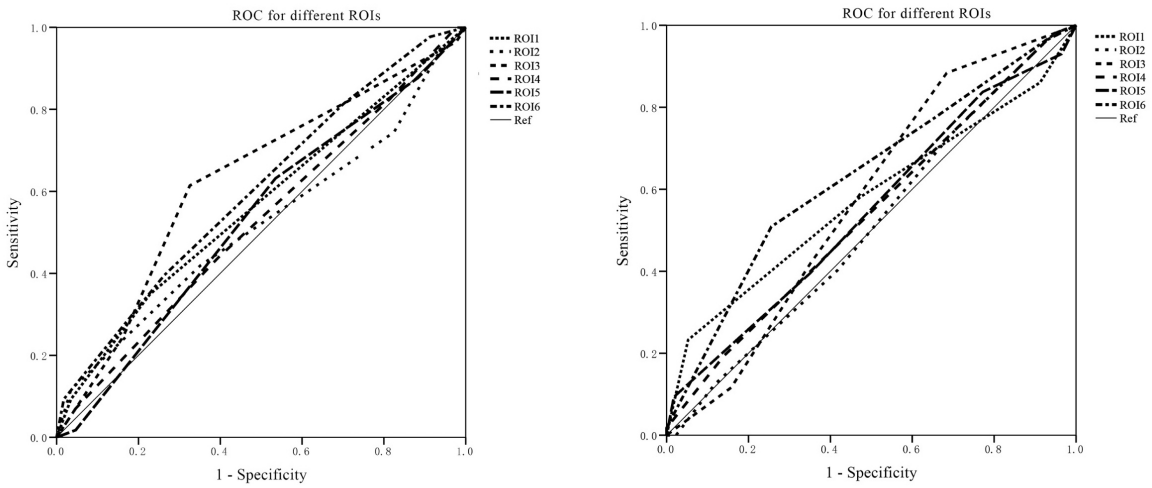

Figure 6. Receiver operating characteristic curve, the plot of the sensitivity vs. (1-specificity) for distinguishing vigilance state in different ROIs.

Table 3. AUC with different ROIs for 'in-degree' and 'out-degree'. In ROI, ROI3, and ROI6, the AUC is significantly higher than that in the other ROIs for 'in-degree' and 'out-degree'.

AUC	ROI1	ROI2	ROI3	ROI4	ROI5	ROI6
in-degree	0.565	0.518	0.626	0.527	0.531	0.601
out-degree	0.575	0.511	0.575	0.541	0.546	0.632

vealed significant differences in positive and negative vigilance states. Among the six ROIs, the considerable gap between 'in-degree' and 'out-degree' based alpha band was observed in ROI3 and ROI6 (p-value below 0.05).

To select the optimal frequency-specific of EEG signals, as discussed above. The alpha frequency band has significant variations in dPDC compared to the other bands. Hence, the next step analyzed based on this step.

3.4 Evaluation of the 'small-world' property for dPDC

Typically, the 'small-world' property exhibits a $C_{real} \gg C_{random}$ for the mean clustering coefficient; and the path length, $L_{real} \approx L_{random}$ (Watts and Strogatz, 1998). The analysis of clustering coefficient *C* and path length *L* of the random and dPDC brain networks was shown in Fig. 7. The results revealed that the clustering coefficients for both groups were higher than those of the random network (the ratios were $\lambda_P = 4.355$ *and* $\lambda_N = 4.385$, respectively). Moreover, the path length was close to (higher than) that of random network (the ratios were $\lambda_P = 1.183$ *and* $\lambda_N = 1.191$, respectively). The 'small-world' configuration of dPDC brain networks shown that the efficiency of information transmission. The clustering coefficients for positive (0.448) and negative (0.451) groups were higher than those of the random network (0.103). And the path length for positive (0.291) and negative (0.294) groups were close to (higher than) that of a random network (0.247). The small-world configuration of dPDC brain networks shown showed that the efficiency of information transmission.

3.5 Classification of different cognitive functions

For single-trial analysis, EEG epochs with a 1 s window and 0.4 s overlap are employed for the dPDC calculation. To analyze the effectiveness of the dPDC-based classification, we compared the performance of the PDC-based network, dPDC-based network, and that of the PLV-based network. Results from the subjects using 10-fold cross-validation were shown in Fig. 8. Overall subjects, the mean classification accuracies obtained are: [PDC] 76.49% [PLV]76.58% [dPDC] 77.69%. On an average, 1.20% and 1.11% classification accuracy improvement for the dPDC-based network

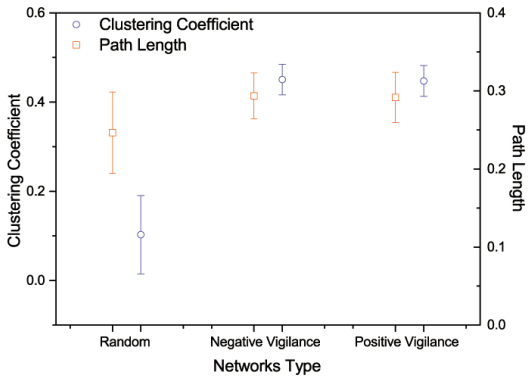

Figure 7. Mean clustering coefficient (blue circle) and path length (red diamond) for the different vigilance state. Error bars correspond to the standard error of the mean. The clustering coefficient and path length for the random networks are used for comparison. The clustering coefficients for positive (0.448) and negative (0.451) groups are higher than those of the random network (0.103). And the path length for positive (0.291) and negative (0.294) groups are close to (higher than) that of a random network (0.247).

can be obtained than PDC-based network and PLV-based network, respectively. The dPDC-based network increased the classification accuracy in 8 out of 13 subjects than others and had a similar performance in 3 out of 13 subjects. Hence, we concluded that the dPDC provided more useful information, and the specific-band effectively improved the classification accuracy compared with the PDC-based network. The PLV-based network provided the network with undirected, while the dPDC-based network provided the directed network.

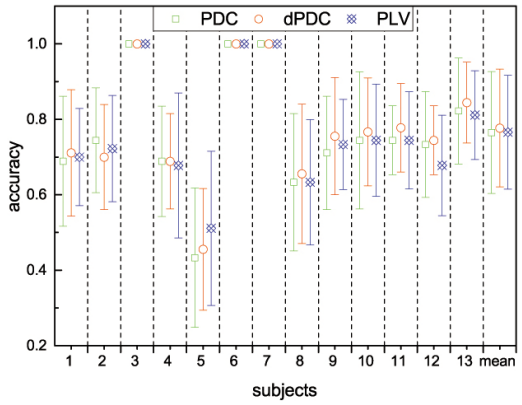

Figure 8. Average classification performance for all 13 subjects and methods. Note that 90% of samples are selected as a training dataset, and the rest of the samples are used for testing. The performance with that of a different network (dPDC-based, PDC-based, and PLV-based network) are analyzed to test and verify the effectiveness of network features.

4. Discussion

The results showed that the proposed method could effectively be used to identify the effective connectivity patterns corresponding to vigilance. In particular, the alpha frequency band and theta frequency band reflect cognition, memory, and age performance (Klimesch, 1999). Following the results presented in Table 1 and Table 2, and it is also the primary reason for the existence of the subject-specific reactive band.

The hit rate was negatively correlated with the overall workload, as measured by the NASA-TLX scores, as shown in Fig. 3. The results showed that the subjects, which had a heavier workload measured by NASA-TLX, had a lower hit rate. Hence, it indicates that the method based on behavior data may be useful to analyze the effectiveness of the experiment.

The network-based dPDC can be used to identify the regions of the brain scalp involved in vigilance since it is rather sensitive to changes in interactions between different regions, as shown in Table 1 and Table 2. The results showed that the differences in the positive and negative vigilance network parameter-based alpha band were significant in ROI1, ROI3, and ROI6 for in-degree and out-degree. Also, the areas under the ROC in ROI1, ROI3, and ROI6, both in-degree and out-degree, were even more extensive than in other brain regions (Fig. 6 and Table 3). The results indicate that the parameters of the network-based alpha band from the fronto-central median, fronto-central right, and parieto-occipital right regions could forecast one's mental vigilance state.

The C for different vigilance states are higher than those of the random network, and the L is close to (higher than) that of a random network. These experimental results show that the effectiveness network has a 'small-world' property, as shown in Fig. 7. It demonstrated that the proposed networks contained 'small-world' features. Compared with PDC-based analysis and PLV-based analysis, the proposed method obtained a slightly better classification result (cf., Fig. 8). This property shows the feasibility of the usage of dPDC to characterize the complexity of brain networks during cognition processing. And the proposed method might be one of the optimal network organization for cognitive processing.

Author contributions

Li YB and Xie SY. conceived and designed the experiments; Li YB performed the experiments and analyzed the data; Li YB wrote the paper; Xie SY revised the paper.

Ethics approval and consent to participate

The Northwestern Polytechnical University approved the research. Informed consent was obtained.

Acknowledgment

This research is funded by the Doctoral Scientific Research Starting Foundation of Xi'an University of Posts and Telecommunications (205020018), the National Science Fund of China under Grant 61273250, in part by the Key Research and Development Program of Shaanxi (2018ZDXM-GY-101), Shaanxi Innovation Capability Support Plan (2018GHJD-10).

Conflict of Interest

The authors declare no conflict of interest.

Submitted: November 11, 2019
Accepted: February 07, 2020
Published: March 30, 2020

References

Ahmadlou, M., Adeli, H. and Adeli, A. (2012) Graph theoretical analysis of organization of functional brain networks in ADHD. *Clinical EEG and Neuroscience* **43**, 5-13.

Akin, M., Kurt, M., Sezgin, N. and Bayram, M. (2008) Estimating vigilance level by using EEG and EMG signals. *Neural Computing and Applications* **17**, 227-236.

Charbonnier, S., Roy, R. N., Bonnet, S. and Campagne, A. (2016) EEG index for control operators' mental fatigue monitoring using interactions between brain regions. *Expert Systems with Applications* **52**, 91-98.

da Fontoura Costa, L. and Sporns, O. (2006) Correlating thalamocortical connectivity and activity. *Applied Physics Letters* **89**, 013903.

Dimitriadis, S. I., Laskaris, N. A., Tzelepi, A. and Economou, G. (2012) Analyzing functional brain connectivity by means of commute times: a new approach and its application to track event-related dynamics. *IEEE Transactions on Biomedical Engineering* **50**, 1302-1309.

Dimitriadis, S. I., Laskaris, N. A., Tsirka, V., Vourkas, M., Micheloyannis, S. and Fotopoulos, S. (2010) Tracking brain dynamics via time-dependent network analysis. *Journal of Neuroscience Methods* **193**, 145-155.

Fagiolo, G. (2007) Clustering in complex directed networks. *Physics and Society* **76**, e026107.

Ferri, R., Rundo, F., Bruni, O., Terzano, M. G. and Stam, C. J. (2007) Small-world network organization of functional connectivity of EEG slow-wave activity during sleep. *Clinical Neurophysiology* **118**, 449-456.

Finomore, V. S. Jr., Shaw, T. H., Warm, J. S., Matthews, G. and Boles, D. B. (2013) Viewing the workload of vigilance through the lenses of the Nasa-Tlx and the Mrq. *Human Factors* **55**, 1044-1063.

Funke, M. E., Warm, J. S., Matthews, G., Riley, M., Finomore, V., Funke, G. J., Knott, B. and Vidulich, M. A. (2010) A comparison of cerebral hemovelocity and blood oxygen saturation levels during vigilance performance. *Human Factors and Ergonomics Society Annual Meeting Proceedings* **54**, 1345-1349.

Gonuguntla, V., Wang, Y. and Veluvolu, K. C. (2016) Event-related functional network identification: application to EEG classification. *IEEE Journal of Selected Topics in Signal Processing* **10**, 1284-1294.

Gorban, A. N. and Zinovyev, A. (2010) Principal manifolds and graphs in practice: from molecular biology to dynamical Systems. *International Journal of Neural Systems* **20**, 219-232.

Hart, S. G. and Staveland, L. E. (1988) Development of NASA-TLX (Task Load Index): results of empirical and theoretical research. *Advances in Psychology* **52**, 139-183.

Keehn, B., Wagner, J. B., Tager-Flusberg, H. and Nelson, C. A. (2013) Functional connectivity in the first year of life in infants at-risk for autism: a preliminary near-infrared spectroscopy study. *Frontiers in Human Neuroscience* **7**, 444.

Klimesch, W. (1999) EEG alpha and theta oscillations reflect cognitive and memory performance: a review and analysis. *Brain Research Reviews* **29**, 169-195.

Laureys, S., Goldman, S., Phillips, C., Van Bogaert, P., Aerts, J., Luxen, A., Franck, G. and Maquet, P. (1999) Impaired effective cortical connectivity in vegetative state: preliminary investigation using PET. *NeuroImage* **9**, 377-382.

Liang, S. F., Lin, C. T., Wu, R. C., Chen, Y. C., Huang, T. Y. and Jung, T. P. (2006) Monitoring driver's alertness based on the driving performance estimation and the EEG power spectrum analysis. In: 2005 IEEE Engineering in Medicine and Biology 27th Annual Conference. 5738-5741.

Neumaier, A. and Schneider, T. (2001) Estimation of parameters and eigenmodes of multivariate autoregressive models. *ACM Transactions on Mathematical Software* **27**, 27-57.

Omidvarnia, A., Azemi, G., Boashash, B., O'Toole, B. J. M., Colditz, P. and Vanhatalo, S. (2014) Measuring time-varying information flow in scalp EEG signals: orthogonalized partial directed coherence. *IEEE Transactions on Biomedical Engineering* **61**, 680-693.

Omidvarnia, A., Mesbah, M., O'Toole, M., Colditz, P. and Boashash, B. (2011) 'Analysis of the time-varying cortical neural connectivity in the newborn EEG: a time-frequency approach', *International Workshop on Systems, Signal Processing and their Applications, WOSSPA*. Tipaza, Algerie.

Rubinov, M. and Olaf, S. (2010) Complex network neasures of brain connectivity: uses and interpretations. *NeuroImage* **52**, 1059-1069.

Stam, C., Jones, B., Nolte, G., Breakspear, M. and Scheltens, P. (2007) Small-World networks and functional connectivity in Alzheimer's disease. *Cerebral Cortex* **17**, 92-99.

Supekar, K., Menon, V., Rubin, D., Musen, M. and Greicius, M. D. (2008) Network analysis of intrinsic functional brain connectivity in Alzheimer's disease. *PLoS Computational Biology* **4**, e1000100.

Watts, D. and Strogatz, S. (1998) Collective dynamics of 'Small-World' networks. *Nature* **393**, 440-442.